Orthopaedic bioactive glass/chitosan composites coated 316L stainless steel by green electrophoretic co-deposition

Zainab M. Al-Rashidy, M.M. Farag, N.A. Abdel Ghany, A.M. Ibrahim, Wafa I. Abdel-Fattah

PII: S0257-8972(17)31199-4
DOI: doi:10.1016/j.surfcoat.2017.11.052
Reference: SCT 22900

To appear in: *Surface & Coatings Technology*

Received date: 1 August 2017
Revised date: 23 October 2017
Accepted date: 18 November 2017

Please cite this article as: Zainab M. Al-Rashidy, M.M. Farag, N.A. Abdel Ghany, A.M. Ibrahim, Wafa I. Abdel-Fattah , Orthopaedic bioactive glass/chitosan composites coated 316L stainless steel by green electrophoretic co-deposition. The address for the corresponding author was captured as affiliation for all authors. Please check if appropriate. Sct(2017), doi:10.1016/j.surfcoat.2017.11.052

Orthopaedic bioactive glass/chitosan composites coated 316L stainless steel by green electrophoretic co-deposition

Zainab M. Al-Rashidy[1], M. M. Farag[2], N. A. Abdel Ghany[3*], A. M. Ibrahim[4], and Wafa I. Abdel-Fattah[1*]

1-Refractories and Ceramics Dept., National Research Centre, Dokki, Cairo, Egypt
2- Glass Research Dept., National Research Centre, Dokki, Cairo, Egypt
3-Physical Chemistry Dept., National Research Centre, Dokki, Cairo, Egypt
4-University College for Girls, Ain Shams University, Cairo, Egypt

***Corresponding authors**:
N. A. Abdel Ghany
Physical Chemistry Dept., National Research Centre, Dokki, 12622, Cairo, Egypt
na_manakhly@yahoo.co.uk, na.abdelghany@nrc.sci.eg

Wafa I. Abdel-Fattah,
Postal address: National Research Centre, Refractories and Ceramics Dept, Tahrir St.,33 El Bohouth St.(former El-Tahrir St.) Dokki, POB 12622, Cairo, Egypt.
E-mail: nrcfifi@yahoo.com

Co-authors:
Z. M. Al-Rashidy
Refractories and Ceramics Dept., National Research Centre, Dokki, 12622, Cairo, Egypt
zmalrashidy@gmail.com

M. M. Farag
Glass Research Dept., National Research Centre, Dokki, 12622, Cairo, Egypt
mmfarag_nrc@yahoo.com

A.M. Ibrahim
University College for Girls, Ain Shams University, Cairo, Egypt
alaa.ellaban@gmail.com

Graphical abstract

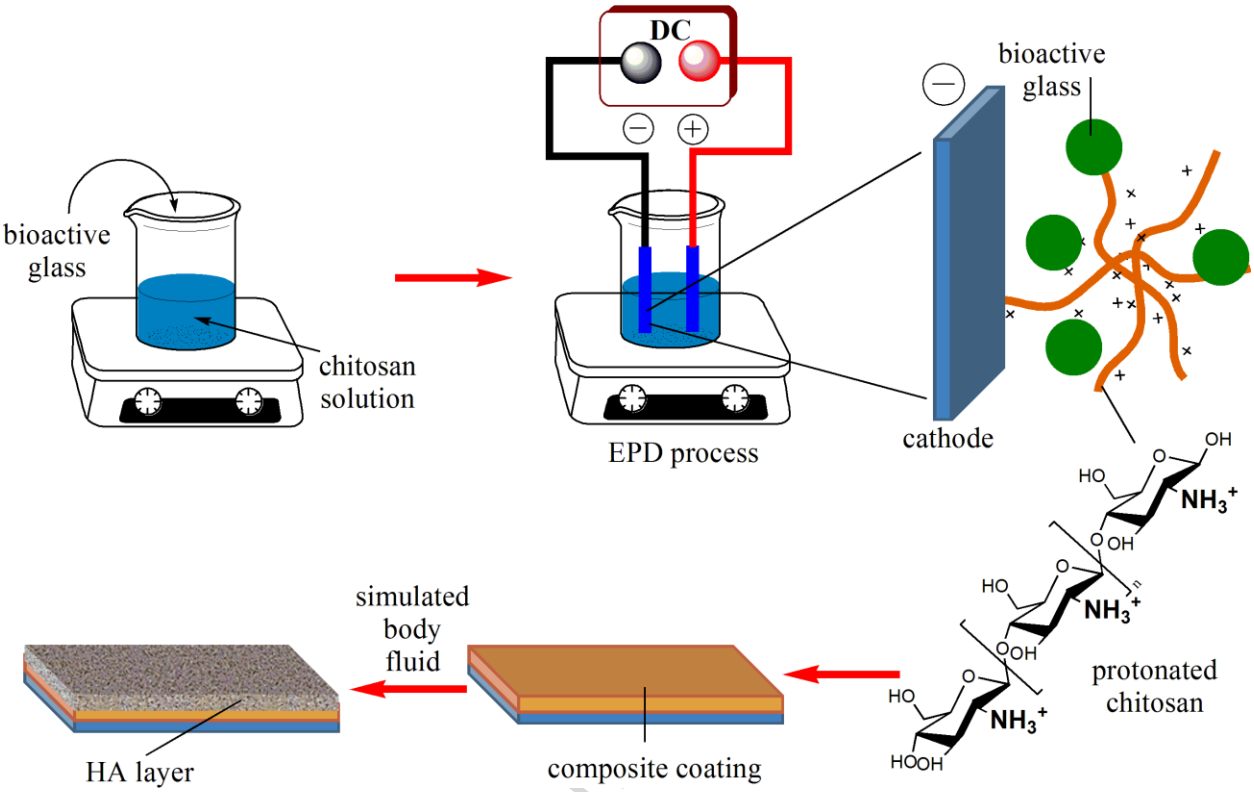

Abstract

Single-step electrophoretic co-deposition (EPD) technique was used to enhance the bioactivity of the 316L stainless steel (316L SS) surface by bioactive glass/chitosan composite coatings. Two modified glass compositions of Bioglass® by the addition of boron were utilized to prepare such composite layers, and the Bioglass® was synthesized for comparison. Different EPD coating factors were studied. Namely, voltage, time, glass powder, and chitosan concentrations, to obtain crack-free and good adhesive coatings. The achieved surfaces were characterized by SEM/EDX, TGA, XRD and FTIR and their wettability and roughness were investigated. The in vitro bioactivity of the coated metals was compared in simulated body fluid (SBF) and Dulbecco's modified eagle medium (DMEM) for up to 15 days. The electrochemical corrosion behavior of the coated metals was evaluated using potentiodynamic polarisation and impedance techniques in the two biological solutions SBF and DMEM at 37 ºC. The results showed that the achieved coatings were uniform, homogenous and crack-free with desirable thickness. Moreover, the coating layers were exhibited by very high wettability, and their roughness values ranged from 170 ± 18 to 234 ± 17 µm. The in vitro bioactivities proved that the coating layers represented a better ability to form hydroxyapatite crystals on their surfaces in SBF than in DMEM. The corrosion resistance of 316L SS was improved by the bioactive composite coatings.

Keywords: glass/chitosan, 316L SS, orthopedic, coating, electrophoretic, corrosion

1. Introduction

Interest significantly increased in the field of coating of metallic implants by bioactive materials. Widely used implants for orthopedic purposes are made mainly of metal alloys, such as stainless steel and titanium alloys. Importantly, 316L stainless steel has been used extensively in the orthopedic field.It is due to its high mechanical strength and low price. Despite the advantages of such metal alloy, it has a shortage in implantation field. Some toxic ions may be released into the body from the metal surface, and the metal is likely encapsulated by fibrous tissue [1, 2], which could lead to the movement and loosening of the metal implant [1, 3]. Nevertheless, a coating of the metal implant surface with bioactive materials has been applied as a practical solution for these problems. Such bioactive layers are characterized by their ability to induce osteointegration of the metal surface, as well as, decreasing or even suppressing the ions released from the metal.

There have been numerous bioactive materials used as coatings for metal implants, such as hydroxyapatite (HA) [4-6], bioactive glass and glass-ceramic [7-10] and composite materials based on biopolymers and ceramic materials [11-14]. Recently, composite inorganic-organic materials have attracted the interest in the orthopedic field. Such materials mimic the bone structure which is composed of collagen as organic phase and nano-HA crystals as the inorganic phase [15]. Therefore, the composite coatings based on biopolymer (as the organic phase, e.g., alginate and chitosan) and ceramic particles (as inorganic phase, e.g., HA and bioactive glasses) combine the bioactivity of the ceramic component and the mechanical properties of the polymer [16]. Furthermore, active biomolecules, such as antibiotics, proteins, and enzymes can be included throughout the polymer matrix during the coating process [16, 17]. Moreover, a room temperature coating process can be achieved by the use of a polymer phase.

Bioactive glasses are an essential class of material for biomedical applications. They can form a chemical bond with surrounding tissue via the formation of HA layer. The bioactive glass was initially discovered by Hench and coworkers in the late 1960's and early 1970's, which was encoded later as 45S5 or Bioglass® [18]. A new research field for using glasses as implants and bone tissue engineering applications was established. After Hench`s glass, other types of bioactive glasses were developed and used in different biomedical applications. Such glasses were widely utilized as bioactive coatings for metal implants. Depending on preparation method, two types of bioactive glass used as a bioactive coating of different metal surfaces; melt-derived

bioactive glasses [8, 19-21] and sol-gel-derived bioactive glasses [22-27]. Nevertheless, the incorporation of boron in bioactive glass compositions proved to enhance the bioactivity and biocompatibility of the glass. Boron showed a potential effect on stimulation angiogenesis in vivo [28], as well as, it proved that it enhanced the growth of bone tissue [29, 30]. Moreover, it was confirmed that boron compounds demonstrated powerful anti-inflammatory effect with minimum side effects [31]. These anti-inflammatory influences come from the defeat of serine proteases that are released by inflammation-activated white blood cells. As well as, boron-containing compounds can reduce the reactive oxygen species which produced in the course of neutrophil's respiratory burst along with T-cell activity [29, 31]. Consequently, the incorporation of boron in bioactive glasses is of particular interest for biomedical applications.

Biopolymers showed a substantial impact on the enhancement of composite coatings properties. Different types of biopolymers were used with bioactive glass particles for coating purpose of metal implants. E.g., polyetheretherketone polymer utilized with 45S5 glass as a composite coating on shape memory alloy (NiTi, Nitinol®) [32]. Furthermore, bioactive glass-alginate composite coatings have been investigated for metal coating application [33]. Moreover, different composite layers based on bioactive glass particles and chitosan have been studied [25, 34-38].

Chitosan has been widely used as an organic component of organic-inorganic composite coatings. It is a natural cationic polysaccharide polymer derived from chitin, which is the second most abundant natural polymer after cellulose. It has numerous advantages to be used in different biomedical applications, such as its antibacterial properties [39]. Additionally, it represented cytocompatibility with varying types of cells [40]. Moreover, desirable mechanical strength, biocompatibility, and biodegradability of chitosan are beneficially controllable [41].

The process of organic-inorganic coatings is a room temperature technique. Following this concept electrophoretic deposition (EPD) in the aqueous electrolyte is considered a superior and green route in this regard. It is characterized by its simplicity being cost-effectiveness with short processing time and achievement of uniform coatings with the possibility for a coat of complex shapes. The EPD process is carried out by passing an electric current between two conductive electrodes immersed in a colloidal suspension. Under an electric field, the particles are charged and moved to the oppositely charged electrode to deposit and co-deposit achieving an adhesive layer on the surface of such electrode [42-45]. EPD technique has been successfully

used to produce composite coatings based on bioactive glass and biopolymers for orthopedic and dental application [32, 34-36, 46].

The present work aimed to prepare composite coatings for 316L SS based on chitosan and new glass compositions using the simple and cost-effective eco-friendly EPD method. The new glasses contained boron, was prepared. Nevertheless, it was targeted to tailor different properties of the suggested composite coatings by changing glass compositions and glass to polymer ratio. Moreover, the surfaces acquired the advantage of chitosan, such as antimicrobial activity, enhancement of the coating adhesion on the metal. Finally, the electrochemical tests of different coated metallic substrates were performed to determine the corrosion behavior of such samples.

2. Experimental procedures

2.1. Materials

The following chemicals with high purity were used in the present work. Chitosan with high molecular weight, 310-375 kDa (Sigma-Aldrich), acetic acid (98%) (Acros Organics, Belgium), SiO_2 (99.8%, quartz sand, Egypt), Na_2CO_3 (99.5%, ADWIC, Egypt), $CaCO_3$ (98.5%, BDH, UK), H_3BO_3 (99.5%, ADWIA, Egypt) and $NH_4H_2PO_4$ (ARABLAB Company, UAE) to fabricate glasses and composites coatings.

2.2. Synthesis of bioactive glass

Table (1) represents glass compositions used in this work in weight percents. Bioglass® (45S5) was synthesized in parallel for comparison. High purity chemicals, SiO_2, Na_2CO_3, $CaCO_3$, H_3BO_3, and $NH_4H_2PO_4$, were used as glass precursors. Glass batch components were mixed well to ensure powder homogeneity. To get rid of the gases resulting from heating the glass components at a temperature above 600 ºC the mixed powders were transformed to a platinum crucible and heated to 1000 ºC in a muffle furnace for one h. After that, the glass batch was melted at temperature range 1350-1450 ºC. The molten glass was poured into water to achieve glass frits. These frits were ground in a ball mill and sieved to get particle sizes less than 63 µm. Moreover, the particle size distribution and zeta potential were evaluated for the achieved glass grains in an aqueous medium using dynamic light scattering analysis (Nicomp N3000

particle size analyzer, Santa Barbara, Calif., USA). The particles were dispersed in the water by sonication probe before the measurement.

Table 1. Three different glass compositions (wt%) used in this study

	SiO_2	Na_2O	CaO	B_2O_3	P_2O_5
40S	40.0	25.0	20.0	5.0	10.0
HB5	40.0	24.5	24.5	5.0	6.0
H	45.0	24.5	24.5	-	6.0

2.3. EPD coating process

A high molecular weight chitosan polymer (0.5, 1.0 or 1.5 g) was dissolved in 1000 ml of 1% acetic acid (98%) solution for one day at room temperature. After complete dissolution of the polymer, glass particles were suspended in the solution by stirring for two hours and sonication (WiseClean, WUC-D03H) for 15 min. Additionally, pH of suspensions was measured.

Stainless steel 316L electrode plates (15 x 10 x 0.2 mm) were polished by 600 and 1200 silicon carbide paper and washed with distilled water and acetone in an ultrasonic bath for 15 min and dried immediately before the electrophoretic coating process. The two electrode coating cell was composed of stainless steel anode and cathode with 1 cm distance with subjected coating area of 10 x 10 mm. Then the two electrodes were immersed in the glass suspension, and an electric voltage was applied by DC power supply (GW Model No: GPC-3060). The samples were carefully and slowly pulled out from the suspension after EPD. Finally, the samples were dried at least for 24 h at ambient conditions.

Different parameters were applied to achieve the optimum conditions for the electrophoretic deposition process. Such parameters for coating were applied voltages (20, 30, 40 and 50 V), time (3, 5, 7, 10 and 15 min.), glass concentrations (2, 4, 6 and 8 g/l), and chitosan concentrations (0.5, 1 and 1.5 g/l). The wt% of the polymer in the composite coating can be calculated from the following equation (1):

$$\text{Polymer wt\%} = Wp * 100/(Wp+Wg) \quad (1)$$

Where, Wp and Wg are the weight of polymer and glass, respectively.

2.3.1. Coating Characterization

Fourier transform infrared spectroscopy (model FT/IR-6100 type A) was used at room temperature (~ 20 ºC) within the wave number range of 4000–400 cm^{-1} at a resolution of 2 cm^{-1}. The functional groups and chemical structure of the prepared borate glass particles and coatings were determined. The thermal behavior of the borate glass was characterized by thermo-gravimetric analysis (TGA) under the nitrogen atmosphere using DSC-TGA instrument model STD Q600 at a heating rate of 10 ºC/min. The surface morphologies and compositions were determined using scanning electron microscopy coupled with Energy Dispersive X-ray analysis (SEM/EDX) (model JEOL JXA-840A, Electron probe microanalyzer). X-ray diffractometer (model, BRUKER as, D8 ADVANCE) was used to study the crystal structure of as-prepared glass and glass coatings using Ni-filtered Cu radiation with a tube voltage of 40 kV. A current of 25 mA was utilized. The wettability of the achieved borate glass coatings was evaluated by measuring the contact angle using horizontal plate camera perpendicular to liquid droplet plane using Compact Video Microscope (CVM), manufactured by SDL-UK. About 250 µl of distilled water was used as a liquid for measuring the wettability according to ASTM D724-99 and ASTM D5946-96 method. Furthermore, the determination of the surface roughness was carried out by Elcometer 224 surface profile meter, UK.

2.4. *In vitro* degradation test

2.4.1. Biological fluids

In vitro degradation tests of the glass-coated substrates were followed in SBF solution which prepared according to Kokubo and Takadama protocol [47] and DMEM solution by measuring the ionic concentrations of the released species from glass coatings and stainless steel substrates. The boron, calcium, phosphorus, silicon, and iron ions along with the total protein levels released into the immersion liquids were measured. The predetermined times of 3, 6, 24, 72, 168 and 336 h using either ICP (model, Agilent5100 Synchronous Vertical Dual View (SVDV)) or colorimetric kits (BIODIGNOSTIC, Egypt)were followed. Ionic boron and silicon concentrations were measured by ICP, and the other ones were measured by colorimetric kits. The pH of incubated solutions was also measured.

2.4.2. Inorganic ionic concentrations

Calcium ions react with methyl thymol, in an alkaline medium to form colored compound (blue color) that absorbed at λ = 585 nm. Inorganic phosphorus reacts with molybdic acid to form phosphomolybdate complex (blue color) that is absorbed at λ = 640 nm. The iron is dissociated by hydrochloric acid then reduced to ferrous by thioglycolic acid. The colored compound which the metal forms with bathophenanthroline was measured colorimetrically at 535 nm. The concentrations of calcium, phosphorus, and iron were calculated by applying the following equation:

$$\text{Concn.} = (A_{sample} / A_{standard}) \text{ x concn. of standard}$$

Where, concentrations of Ca and P ions were in mmol/l and concentration of Fe ion was in µmol/l.

The protein molecule when treated with an alkaline cupric sulphate, form a violet colour that absorbs at 550 nm. The concentration of protein is calculated by the following equation:

$$\text{Concn.} = (A_{sample} / A_{standard}) \text{ x } 5 \quad \text{g/dl}$$

2.4.3. Corrosion behaviour evaluation

The electrochemical behavior of both the uncoated and coated substrates in SBF and DMEM solutions were investigated by potentiodynamic polarisation test, and electrochemical impedance spectroscopy (EIS). Before each test, the specimen's surface area of the working electrode that contact with the electrolyte was cleaned and the working area was measured. The electrochemical three-electrode cell was used for in vitro potentiodynamic corrosion tests. The platinum sheet was used as a counter electrode and saturated calomel electrode (SCE) as a reference electrode. SBF and DMEM solutions were used as an electrolyte to evaluate and compare the corrosion behavior of 316L SS with and without composite coating. The potentiodynamic polarization experiments were run; where each of 316L SS substrate and composite coated 316L SS samples were immersed for 15 min in physiological solutions at the temperature of 37 ◦C before measurement to attain the steady state potential. Potentiodynamic polarisation curves were performed using Autolab 302N electrochemical workstation (Metrohm). Dynamic polarisation curves were recorded at a potential scanning rate of 1 mV/S, at open air. The reversed current density for cyclic polarisation was one mA/cm^2.

The anodic and cathodic polarisation curves were obtained for each specimen starting from steady-state potential. The corrosion current density, corrosion rate and corrosion potential

of various samples (316L SS substrate and composite coated 316L SS samples) were determined by Tafel extrapolation. For reducibility, five sets of the uncoated and coated samples obtained under the optimum coating parameters were measured.

The electrochemical impedance spectroscopy (EIS) data were recorded from 20 kHz to 0.01 Hz with a ten mV sinusoidal perturbing signal at open-circuit potential. To reduce the time and potential noise interference the lowest frequency was set to 0.01 Hz. The EIS measurement may be affected by phase shifts from the potentiostat in the high-frequency region, and so the upper-frequency limit was set at 20 kHz. In this method, the samples were immersed in SBF and DMEM solutions at 37 ± one ºC. In the analysis of the impedance data, the appropriate equivalent circuit EC which did not only match the physical structure of measured electrode system but was also able to produce similarly proposed spectrum diagrams for the examined samples.

2.5. Statistical analysis

All experimental data stated in this work were expressed as the average ± standard deviation (SD) for n = 3 and were analyzed using standard analysis of Student's t-test. The level of significance (P value) is set at < 0.05.

3. Results and discussion

3.1. Glass characterization

Figure 1a represents XRD patterns of the as-casted three glass samples (the 40 S, Ws, HB5, and H). The figure shows no diffraction peaks for all the samples, which proved their amorphous structure. Moreover, the particle sized distribution analysis was carried out for glass particles used in EPD coating process which showed in Figure 1b. The figure showed a monomodal, and narrow particle size distribution for all glasses ranged from 0.3 µm to 10 µm. Three cumulative % points (D10, D50, and D90) were used herein to represent the extremes and the mean particle sizes (Table 2). The size diameters, D10 of 0.47, 0.49 and 0.44 µm, and D90 of 2.63, 1.77 and 2.10 µm were measured for the 40s, HB5 and H samples, respectively. Moreover, D50 was represented the mean particle size distribution were measured for the 40s, HB5 and H samples as 1.37, 1.10 and 1.20 µm, respectively. On the other hand, the zeta potential of different glass particles was measured in an aqueous medium (Table 2). The results showed that H glass

(Bioglass®) particles demonstrated higher negatively charged particles (-41.13 mV) than the 40s (-18.63 mV) and HB5 (-24.78 mV) glass particles in an aqueous medium. These likely attributed to higher SiO_2 wt% in H glass and consequently higher number of silanol groups which created in aqueous solution on the glass surface as a result of non-bridging oxygens hydration of Si-O groups in glass network.

Table 2. Different cumulative % points of particle size (µm) and zeta potential (mV) of different glasses

	Cumulative % point of diameter (µm)			Zeta potential (mV)
	D10	D50	D90	
40S	0.47	1.37	2.63	-18.63
HB5	0.49	1.10	1.77	-24.78
H	0.44	1.20	2.10	-41.13

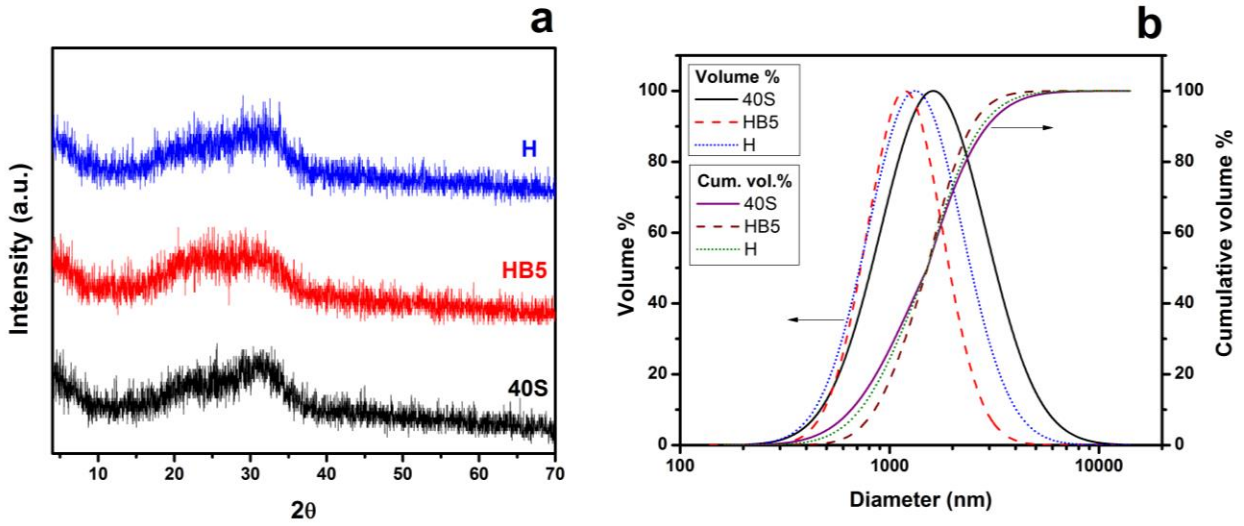

Figure 1. XRD patterns (a) and particle size distribution (b) of as-prepared glass particle (40S, HB5 and H).

3.2. Effect of different coating parameters

The chitosan solutions containing glass particles were deposited on the cathode electrode. As chitosan polymer is dissolved in an acidic medium, it becomes a cationic polyelectrolyte at pH < 5 because it can be protonated and so it gains a positive charge as shown in Figure 2 [48]. As mentioned before from zeta potential measurements, all glass particles showed negatively charged particles in the aqueous medium. Therefore, attraction forces can be created between

these negatively charged glass particles and positively charged chitosan, and consequently, each glass particle was likely surrounded by chitosan layer and formed the stable suspension.

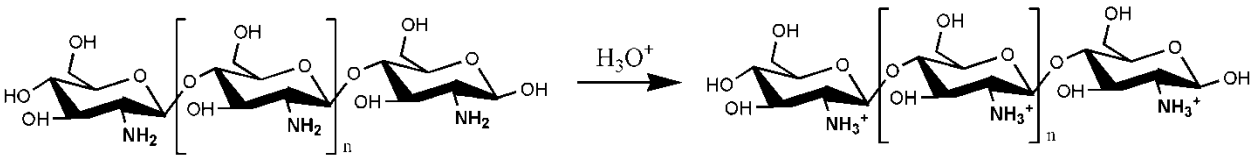

Figure 2. Protonation of chitosan polymer in acidic medium

A variety of different factors of the coating process did not change the deposited electrode. Therefore, the deposition of composite coating depended mainly on the chitosan polymer that was because the chitosan shifted the zeta potential of glass particles to the positive value. These results agreed with the previous study [49]. Nevertheless, several coating conditions of voltage, coating time, glass, and polymer concentrations were examined to achieve good adhesive, homogeneous and crack free coatings with desirable thickness. The results showed that the composite layers were produced successfully at optimum conditions of; 20 V, deposition time of 5 min, 0.5 g/l polymer concentration and 6 g/l glass concentration. Any lower values of these parameters produced inhomogeneous and thin layers, while, higher ones resulted in thick and bad-adhesive, extraordinarily porous and easily cracked coatings. On the other hand, pH values measured for chitosan solution and glass/chitosan suspension were 3.43 for chitosan solution, 4.77, 4.75 and 4.67 for suspensions contained the 40s, HB5 and H glass particles, respectively. Therefore, different glass suspensions possessed pH < 5, and accordingly, chitosan was remained protonated and acquired a positive charge, which enhances the deposition on the cathodic compartment during EPD process.

3.3. Thermogravimetric analysis (TGA)

The thermogravimetric analysis (TGA) of as-prepared glass and the three derived composite coatings (40S, HB5 and H samples) in the temperature range 25-900 $^{\circ}$C is presented in Figure 23. The weight loss values of as-prepared glasses were very low and they did not exceed 5% up to 850 °C. Such weight loss can be attributed to the loss of adsorbed water molecules on the surface of glass particles. Nevertheless, the weight loss of as-prepared glass particles

followed the order H > 40S > HB5, which likely attributed to the water adsorption affinity of each glass type. Moreover, the recorded weight loss of the composite coatings can be ascribed to the evaporation of the adsorbed water molecules on the coatings, as well as, the thermal decomposition of chitosan backbone. It can be observed from the figure that the weight loss occurred in two steps for 40S (at temperature ranges; 25-230 ºC and 230-550 ºC) composite sample, while it occurred in four steps for the HB5 (at temperature ranges; 25-146 ºC, 146-228 ºC, 228-650 ºC and 650-700 ºC) and H (at temperature ranges; 25-146 ºC, 146-230 ºC, 230-580 ºC and 680-640 ºC) composites. The total weight loss for the 40S, HB5 and H, was 28.5%, 25% and 31.5%, respectively. Consequently, the glass content was 71.5%, 75% and 68.5%, respectively. Interestingly, the weight loss order of composite coatings was the same order for the corresponding glasses. However, the experimental weight losses were ranged from 25% to 31.5% which were higher than the theoretical starting chitosan polymer (~7.7 %) calculated according to Equation (1). This difference might be originated from the evaporation of water molecules adsorbed on the glass particle surfaces and that incorporated into the chitosan polymer. From the other side, during the EPD process, precipitation of glass particles was occurred to some degree, which affected the final glass-to-polymer weight ratio.

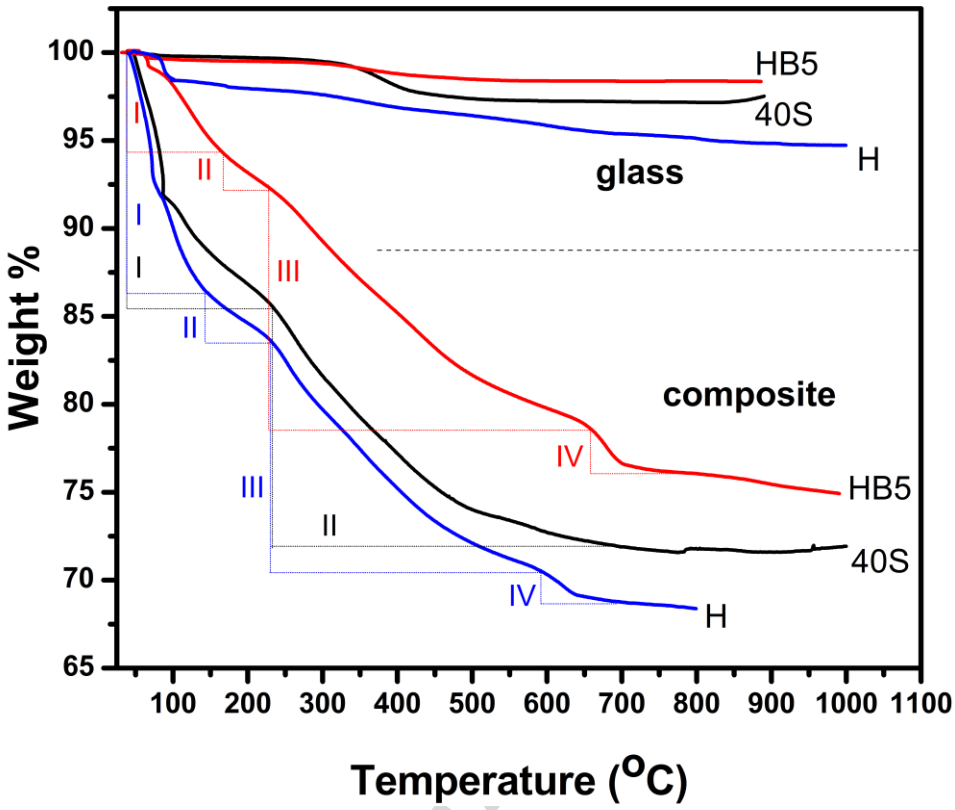

Figure 3.Thermogravimetric analysis (TGA) of as-prepared glass and the derived composite coatings (40S, HB5 and H samples).

3.4. SEM-EDX analysis of coated substrates

Figure 4 represents SEM micrographs of the metal coated surface (upper), its cross section (middle) and EDX analysis (lower) of the 40s, HB5 and H composite coating samples. The figure for all composite coatings showed that the glass particles were dispersed homogeneously within the chitosan matrix. Moreover, suitable adhesive and crack-free layers are demonstrated. Nevertheless, the composite coating thicknesses measured from SEM micrographs varied according to the type of glass filler. H sample showed larger coating thickness (246 ± 47 µm) than HB5 (105 ± 16 µm) and 40S (143 ± 33 µm) samples. Again, these differences in the coating thicknesses were likely assigned to the difference of zeta potential of the three glass powders in an aqueous medium. A higher negative charge of H glass can be prospective formed a more stable suspension which achieved optimal conditions for depositing a thicker layer. Moreover, high roughness morphologies of the coating surfaces were recorded from the cross-section of the samples and high standard deviation values of thickness measurements. On the

other hand, EDX analyses of different coating surfaces showed the same elemental components of the glass particles.

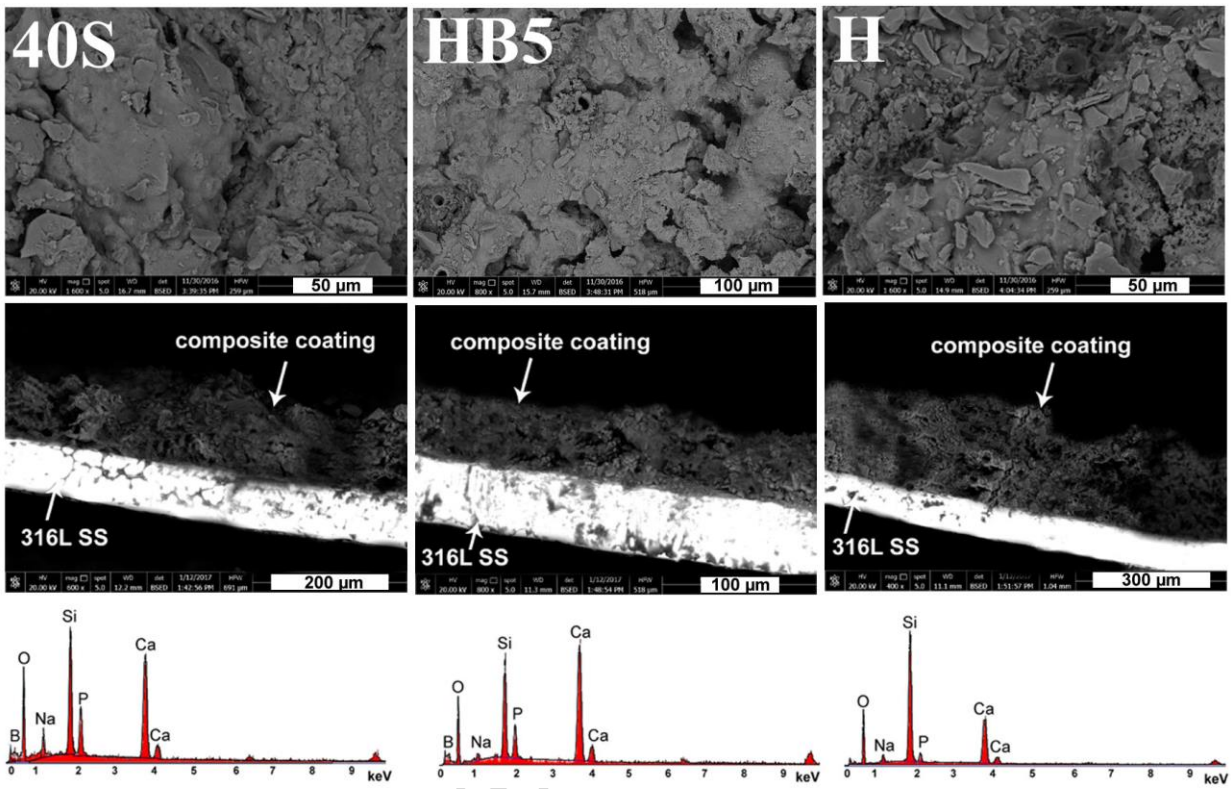

Figure 4. SEM micrographs of metal coated surface (upper) and its cross section (middle) and corresponding EDX analysis (lower) for the surfaces of40S, HB5 and H composite coatings.

3.5. Wettability and roughness of coated substrates

The wettability of the bioactive coatings for metal implants is essential issues from the view of cell viability principle. The hydrophilic surface of bioactive materials is one of the crucial marks for cell attachment and proliferation on such surface [50]. The wettability is measured from the contact angle between the tangent of a water drop and substrate plane. Figure 5 demonstrates optical photos of water drop before (upper) and after (lower) contacting with the different coated metal substrate surfaces (the 40s, HB5 and H samples). The figure showed that it was not possible to measure the contact angle because the water drop wholly diffused and absorbed by the coating surface, it was almost zero. This result indicated the high wettability of composite coating layers, which mainly resulted from the hydrophilic nature of chitosan polymer and bioactive glass particles. These results agreed with a previous study [51]. Interestingly, the

new glasses (the 40s and HB5 glasses) prepared in this study had hydrophilic properties like 45S5 glass. Therefore, different composite coatings transformed the substrate surface to be wholly wettable and the hydrophilic surface giving a positive mark for the cell attachment and interaction [50].

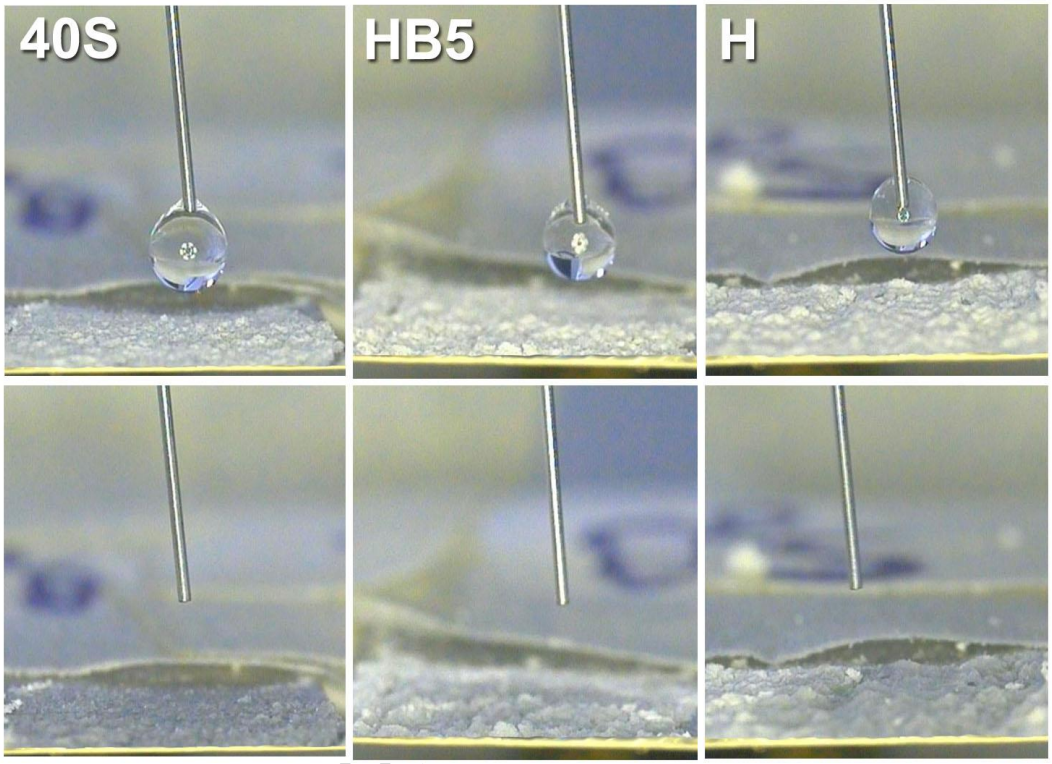

Figure 5. Optical photos of water drop before (upper) and after (lower) contacting with different coated metal substrate surfaces, 40S, HB5 and H samples.

Figure 6 represents the average roughness values of the composite coatings compared to 316L SS substrate. The roughness values of 316L SS, the 40s, HB5 and H composite coatings were five ± 0.7, 170 ± 18, 234 ± 17 and 201 ± 26 µm respectively. All the coats ($P << 0.01$) increased the roughness of 316L SS significantly. HB5 sample showed substantially higher roughness than the 40s and H samples acquiring values of $P \sim 0.0001$ and 0.03, respectively.The 40S sample possessed lower value than each HB5 and H samples ($P \sim 0.0001$ and 0.04, respectively). The coatings showed micro-topographies which enhances cell adhesion as demonstrated in a previous study [52]. In other words, the samples demonstrated desirable roughness which can be advantageous for bioactivity, where it promotes an adsorption of organic components and enhance the cell attachment inside the body.

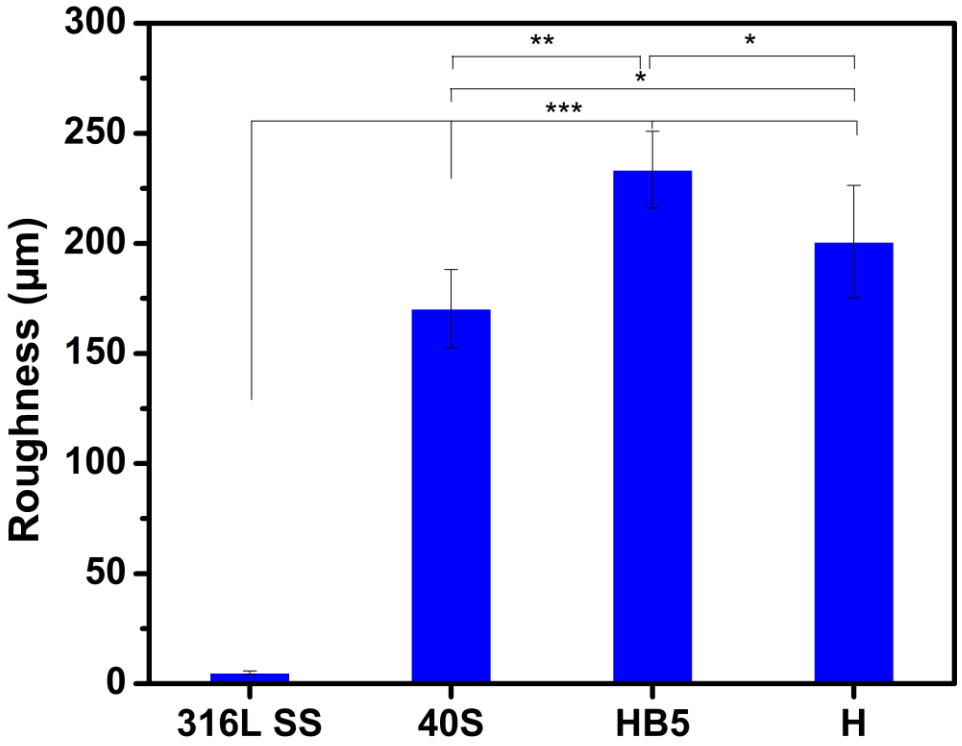

Figure 6. Roughness values of different composite coating compared to 316L SS substrate. P-value obtained by Student's t-test (*P<0.05, **P< 0.01 and ***P<1x10^{-7})

3.6. *In vitro* degradation and bioactivity tests

3.6.1. pH measurements

The pH of the incubated media (SBF and DMEM) of the studied composite coated substrates as a function of time are represented in Figure 7a, b. The pH values of samples after immersion in SBF reached its maximum values ranging from 7.4 to 7.5 after one-day incubation, and then they decreased continuously throughout the rest of incubation period to reach to values around 7.0. Such decrease is attributed to the depletion of Ca and P ions present in SBF for the hydroxyapatite crystals formation as confirmed by the degradation curve of Ca and P ions (Figures 6c and d). On the other hand, pH values of samples incubated in DMEM showed different behavior, where, fluctuation of pH values was recorded. pH values reached their maxima to become around 8.0 post six h of incubation, and then they decreased to their minimum values to reach 7.1 after three days of immersion. Further, they increased again and continuously during the rest of the immersion time to reach values between 7.4 and 7.9. Such variation in pH values was due to the non-buffered nature of such fluid (unlike SBF) [53].

3.6.2. Ionic release concentrations

The levels of Ca, P, Si, B, Fe and total proteins released from different composite coatings into SBF and DMEM are shown in Figures 6 c-l. Mostly, the release of all ions in SBF and DMEM showed a two-stage release. The first stage occurred in the first day of in incubation and it showed a relatively high release rate. The second stage was steady state release which occurred during the rest of soaking time (1-14 d), and it characterized by a lower release rate.

Figures 7c and d represent the cumulative release curves of Ca ion in both solutions. Generally, Ca ions concentration in SBF was slightly higher than that in DMEM solution. This was because of a higher initial Ca ionic concentration in SBF (2.5 mmol/dm^3) compared to that in DMEM (1.8 mmol/dm^3) [53]. On the other hand, the concentration of Ca ions in SBF was increased during the first day of incubation with rates 20.0 x 10^{-2}, 21.4 x 10^{-2} and 22.2 x 10^{-2} mmol/l.h^{-1} for 40S, HB5 and H samples, respectively. Thereafter, the release rates were decreased throughout the rest of incubation period with rates 1.7 x 10^{-2}, 1.7 x 10^{-2} and 1.9 x 10^{-2} mmol/l.h^{-1}. As mentioned before, Ca ions leached out from glass particles increased to some extent their concentration in the solution. Such leached ions; besides original Ca ions in SBF were utilised in the formation of bone-like apatite layer, which in turn decreased Ca ions concentration in the fluid. Then again, H sample showed more released amount of Ca ions in SBF than 40S and HB5 samples. This can be attributed to a higher wt% of CaO in H glass (24.5 wt%) than in 40S glass (20 wt%). Despite the percentages of CaO in H and HB5 glasses were the same, the amount of released Ca ions in the fluid incubating H sample was higher than that incubating HB5 one. This might be due to the substitution of silicon by boron which strengthens the glass network and then decreased the degradation of the glass filler. As it was demonstrated in previous studies, boron could strengthen the silicate framework of borosilicate glass, and then increase its chemical durability [42]. On contrary, the concentrations of Ca ion in DMEM for all samples, and the release rates were similar to the release rates in SBF. Where, they increased during the first day of incubation with rates 17.7 x 10^{-2}, 17.2 x 10^{-2} and 17.6 x 10^{-2} mmol/l.h^{-1} for 40S, HB5 and H samples, respectively, and they similarly decreased during the rest of incubation time to become around 1.6 x 10^{-2} mmol/l.h^{-1} for three samples.

Figures 7 e and f show the cumulative release profiles of P ion in SBF and DMEM solutions. In the case of incubation in SBF, the concentrations of P ions increased initially during the first day of incubation, the recorded release rates for 40S, HB5 and H samples were 6.7 x 10^{-}

^{2}, 6.2 x 10^{-2} and 6.1 x 10^{-2} mmol/l.h^{-1}. However, the release rates of P ions decreased through the rest of soaking time and they became around 0.7 x 10^{-2} mmol/l.h^{-1} for whole samples. This initial increase in P ion concentrations can be attributed to the release of P ions from the glass surfaces followed by a decrease in the release rate due to the expenditure of P ions in the formation of bone-like apatite crystals. These results agreed with previous work [54]. Besides, the concentration of P ions in the fluid incubating 40S sample was higher than that incubated HB5 and H samples. Similarly, this result is assigned to the original higher percentage of phosphate component in 40S glass (10 wt%) than the other two glasses (both glasses had the same percentage, 6 wt%). In contrast, the dissolution curves of different samples in DMEM exhibited higher release rates of P ions (8.9 x 10^{-2}, 9.3 x 10^{-2} and 9.3 x 10^{-2} mmol/l.h^{-1} for 40S, HB5 and H, respectively) than that in SBF in the first day, but, the release rates were similar to the release rates in SBF.

The cumulative concentrations of Si ions released from different composite coatings are represented in Figures 7g and h. from the figure it was noted that the concentration and the rates of Si ions released into SBF (11.6 x 10^{-2}, 8.1 x 10^{-2} and 10.1 x 10^{-2} mmol/l.h^{-1} for 40S, HB5 and H, respectively) were lower than that released in DMEM (15.3 x 10^{-2}, 13.1 x 10^{-2} and 10.1 x 10^{-2} mmol/l.h^{-1} for 40S, HB5 and H, respectively). Thereafter, the release rates were decreased during the rest of soaking time to become 0.8 x 10^{-2}, 0.7 x 10^{-2} and 0.9 x 10^{-2} mmol/l.h^{-1} in SBF and 1.9 x 10^{-2}, 1.3 x 10^{-2} and 1.8 x 10^{-2} mmol/l.h^{-1} in DMEM for 40S, HB5 and H, respectively. This can be attributed to Na ion leaching from glass surface, which was followed by breaking of Si-O-Si bond generating non bridging oxygen that was easily leached out and hydrolyzed by water to form silanol groups (Si-OH) on the glass surface, and consequently increased the Si ions concentration in initial soaking time. Additionally, in the bioactive glasses related to Hench glass (45S5 glass), small silicate species may be released without the hydrolysis step [55]. In such case, the formation of silanol layer after a certain time on the glass surface can be acting as a protective layer to suppress the dissolution of silicate units which explaining the decrease of Si concentration after reaching its maximum. On the contrary, the concentration trend of Si ions in DMEM was higher due to the corrosive properties of this solution. Furthermore, the trend of B dissolution was similar in both solutions (Figures 7 i and j). It increased abruptly throughout the first day of incubation period with rates of 5.5 x 10^{-2} and 6.6 x 10^{-2} mmol/l.h^{-1} in SBF and 6.6 x 10^{-2} and 4.9 x 10^{-2} mmol/l.h^{-1} in DMEM for 40S and HB5, respectively. And then, they became

almost constant (0.09 x 10^{-2} and 0.12 x 10^{-2} mmol/l.h^{-1} in SBF and 0.10 x 10^{-2} and 0.07 x 10^{-2} mmol/l.h^{-1} in DMEM for 40S and HB5, respectively) during the rest of immersion time due to the formation of hydroxyapatite layer on the composite coatings.

Figures 7 k and l represent the dissolution profiles of Fe ions in SBF and DMEM solutions. The figure showed that the rate of release of Fe ions in both solutions decreased after 1 day of immersion time. They were 46.6 x 10^{-2}, 48.1 x 10^{-2} and 60.1 x 10^{-2} µmol/l.h^{-1} in SBF and 40.4 x 10^{-2}, 51.3 x 10^{-2} and 38.2 x 10^{-2} µmol/l.h^{-1} in DMEM for 40S and HB5, respectively during the first day of incubation, and they decreased to 5.8 x 10^{-2}, 5.9 x 10^{-2} and 7.4 x 10^{-2} µmol/l.h^{-1} in SBF and 3.9 x 10^{-2}, 6.4 x 10^{-2} and 5.3 x 10^{-2} µmol/l.h^{-1} in DMEM for 40S and HB5, respectively, throughout the rest of immersion time. The decrease of Fe ion release rates in SBF and DMEM can be ascribed to the formation of hydroxyapatite crystals on the composite coatings which reduced the penetration of water molecules to metal/composite interfaces. Therefore, the composite coatings showed an unusual anticorrosion behavior in SBF and DMEM solutions, and they indicated their remarkable role to protect the metal substrates from initiation of corrosion reaction in different fluids.

Figure 7m shows the change of cumulative concentration of total proteins in DMEM solution during the incubation of 40S, HB5 and H samples. It is obvious that the concentrations of the total proteins obviously increased initially on the first day of incubation with rates of 9.4 x 10^{-2}, 9.7 x 10^{-2} and 11.3 x 10^{-2} g/dl.h^{-1} for 40S, HB5 and H, respectively, followed by a decrease in release rate during the rest of immersion time (1.1 x 10^{-2}, 1.1 x 10^{-2} and 1.0 x 10^{-2} g/dl.h^{-1} for 40S, HB5 and H, respectively). The initial increase of total proteins concentration was likely due to the degradation of chitosan polymer matrix. The degradation can be occurred mostly by the random cleavage of β-1,4-glycosidic bonds followed by N-acetyl linkage (deacetylation) [56], this degradation process produced small chains of oligosaccharides and destruction of chitosan functional groups (amido, carbonyl, hydroxyl and amino groups). These produced fragments can be recombined and form some kinds of amino acids which can be detected during the total protein analysis. However, the concentration of the proteins in DMEM decreased through the rest of soaking time can be attributed to re-adsorption of the proteins already present in the solution on the coating surface.

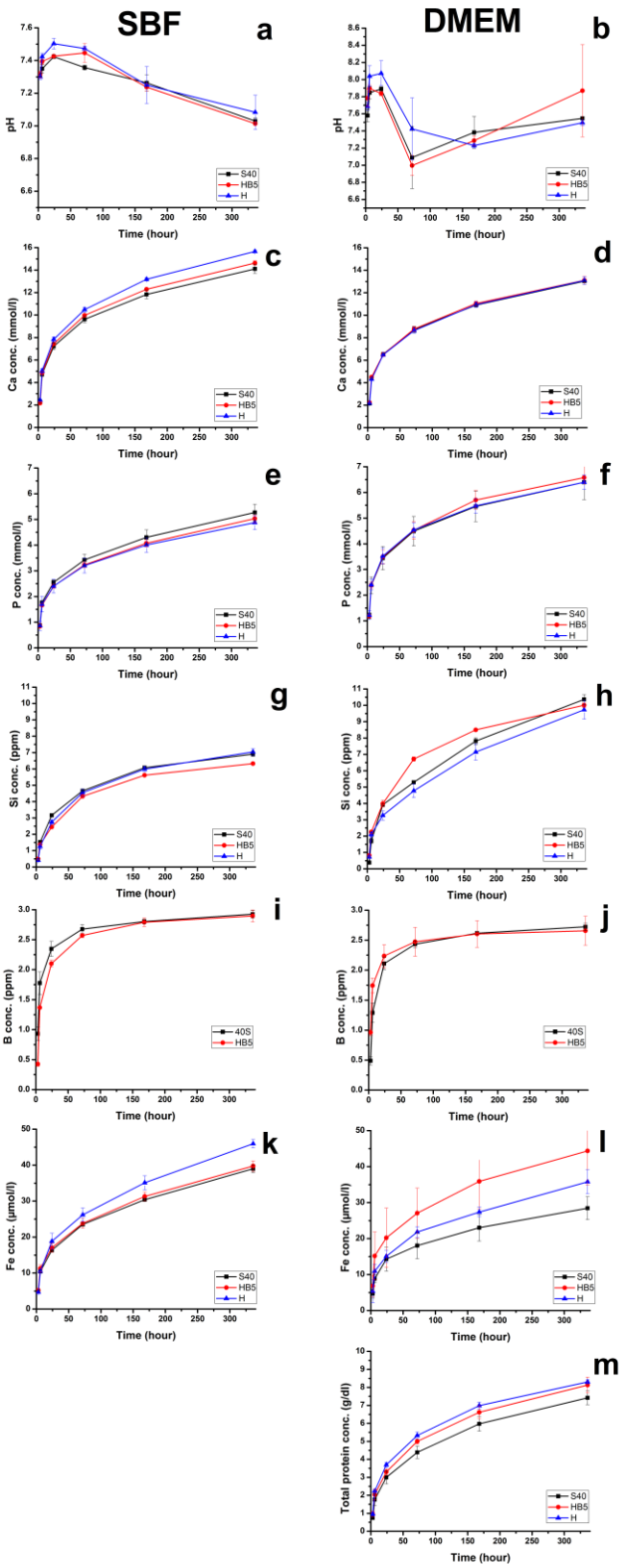

Figure 7. pH change (a & b) and the cumulative concentration of released Ca (c & d), P (e and f), Si (g & h), B (i & j) and Fe (k & l) in SBF and DMEM solutions, respectively; and total released proteins (m) into DMEM as a function of time.

3.6.3. In vitro assessment in SBF

Figure 8 represents SEM and EDX analyses of different metal coated substrates after immersion in SBF at 37 ºC for 14 days. The known HA agglomerated crystals were observed on the surfaces of the different coatings in SEM micrographs. The evident increase of Ca and P observed in EDX analysis confirmed the formation of Ca phosphate crystals on the composite coatings. The atomic Ca/P ratio was calculated roughly from EDX analysis; it was 2.52, 1.41 and 3.34 for 40S, HB5 and H samples, respectively. This result agreed with Ca and P ions concentration in SBF, possessed a decreased release rate after the first day of the incubation period because they depleted due to the formation of the bone-like apatite layer.

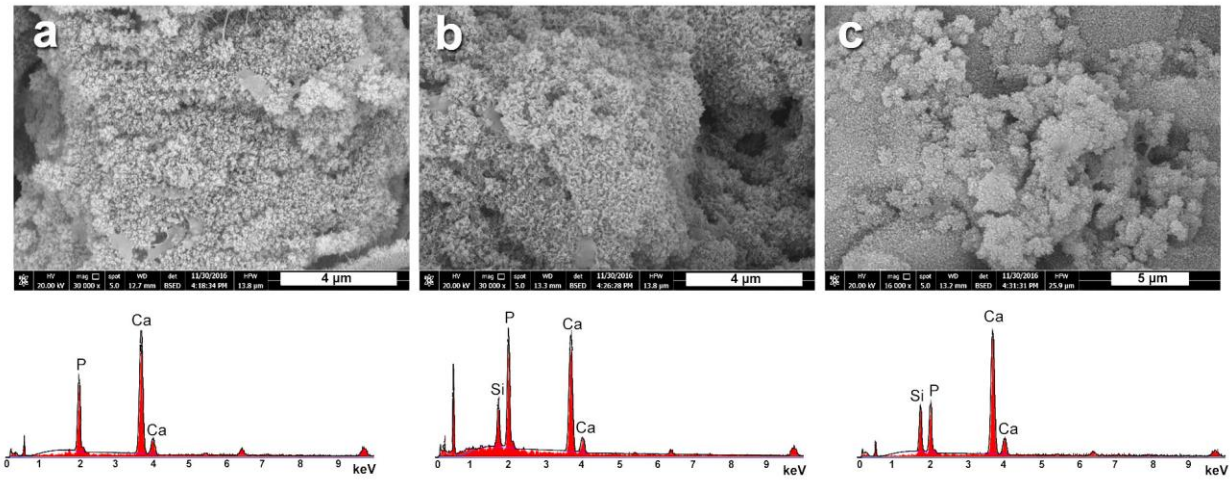

Figure 8. SEM micrographs and EDX analysis of 40S, HB5 and H composite coatings (a, b and c, respectively) after immersion in SBF for 14 days.

3.6.4. IR analysis after immersion in SBF and DMEM

Figure 9 represents FTIR spectra of the 40s, HB5 and H of the surfaces of metal composite coatings post-immersion in SBF and DMEM at different times. The characteristic peaks of the composite components (silicate-based glasses and chitosan) beside Ca phosphate (mainly HA) bonds are proved. Some residual bands were observed for chitosan polymer, where the relatively sharp and big vibration bands centered at about 1647 cm^{-1} were assigned to a combination of vibration modes of the amide groups in chitosan. Moreover, two reflection bands at about 1142 and 863 cm^{-1} were attributed to the stretching vibration modes of C-O-C groups of the polysaccharide structure of chitosan [57]. New characteristic bands for Ca phosphate bonds were detected. Stretching vibrations of PO_4^{3-} were identified at 560 and 605 cm^{-1}. Moreover,

vibration bands of carbonate group at 870 and 1420 cm^{-1} confirmed a formation of newly carbonated HA layer. Furthermore, bands observed at 450, 791 and 1647 cm^{-1} (interfered with OH vibration mode in water molecules) were attributed to the silanol group in Si-O-Si bands [58]. However, the vibration bands of Ca phosphate bonds were more evident in SBF than DMEM. This can be explained by the complex composition of DMEM, where it contained some kinds of proteins (proteins kinds) which likely inhibit the formation of HA layer on bioactive materials. Organic components contained in the DMEM solution failed to prevent the formation of crystalline phases [53].

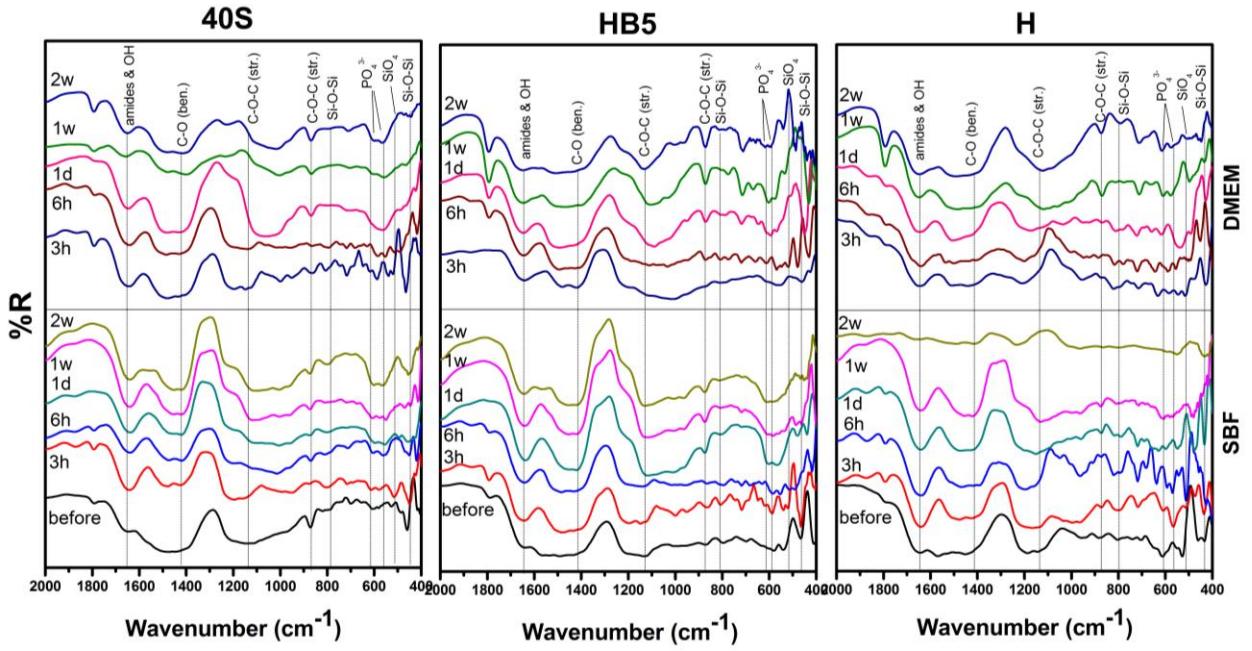

Figure 9. FTIR spectra of 40S, HB5 and H of the surfaces of metal composite coatings before and after immersion in SBF and DMEM at different times.

3.7. Electrochemical measurements

3.7.1. Potentiodynamic polarization

The potentiodynamic polarisation curves of the uncoated substrate and coated samples (the 40s, HB5 and H) in SBF and DMEM solutions are shown in Figures 10 a and b. Measurements were repeated several times, and the adopted curves represent the nearest to the mean measured values. Accordingly the values of the corrosion current density (I_{corr}) , corrosion potential (E_{corr}) of each group of 316L SS and coated samples which are shown in Table 3 and

Figure 10. Figure 10 represented that the uncoated sample has a reasonably negative corrosion potential in SBF and DMEM of about -424.5 mV and -436 mV, respectively. The corrosion potential of the coated samples was nobler and shifted to approximately -380.5, -371.8 and -281.9 mV for the 40s, HB5, H composites coatings in SBF, respectively. A similar trend observed in the DMEM solution and the values of the 40s, HB5 and H samples were -397.9, -312.4 and -285.3 mV, respectively. It was also observed that the corrosion current density and corrosion rate of the coated samples in SBF and DMEM solutions were lower than that of the uncoated substrate, proving, therefore, a much smaller corrosion rate on the coated sample. Based on these experimental results, the glass/chitosan composite coatings can indeed improve the corrosion resistance of 316L stainless steel significantly [59, 60].

Table 3. Mean values of corrosion current densities and corrosion potentials of uncoated SS and composites coated samples in physiological solutions at 37 ± 1 ◦C.

Electrolytes / Coatings	SBF			DMEM		
	Corr. Rate mpy	**E_{corr} (mV)**	**I_{corr} (µA/cm^2)**	**Corr. Rate, mpy**	**E_{corr}, (mV)**	**I_{corr}, (µA/cm^2)**
316SS Blank	**13.85**	**-424.5**	**30.48**	**10.39**	**-436**	**22.86**
40S	5.022	-380.5	20.93	5.319	-397.9	13.35
HB5	7.752	-371.8	17.06	2.19	-312.4	7.1
H	8.543	-281.9	18.72	2.764	-285.3	7.07

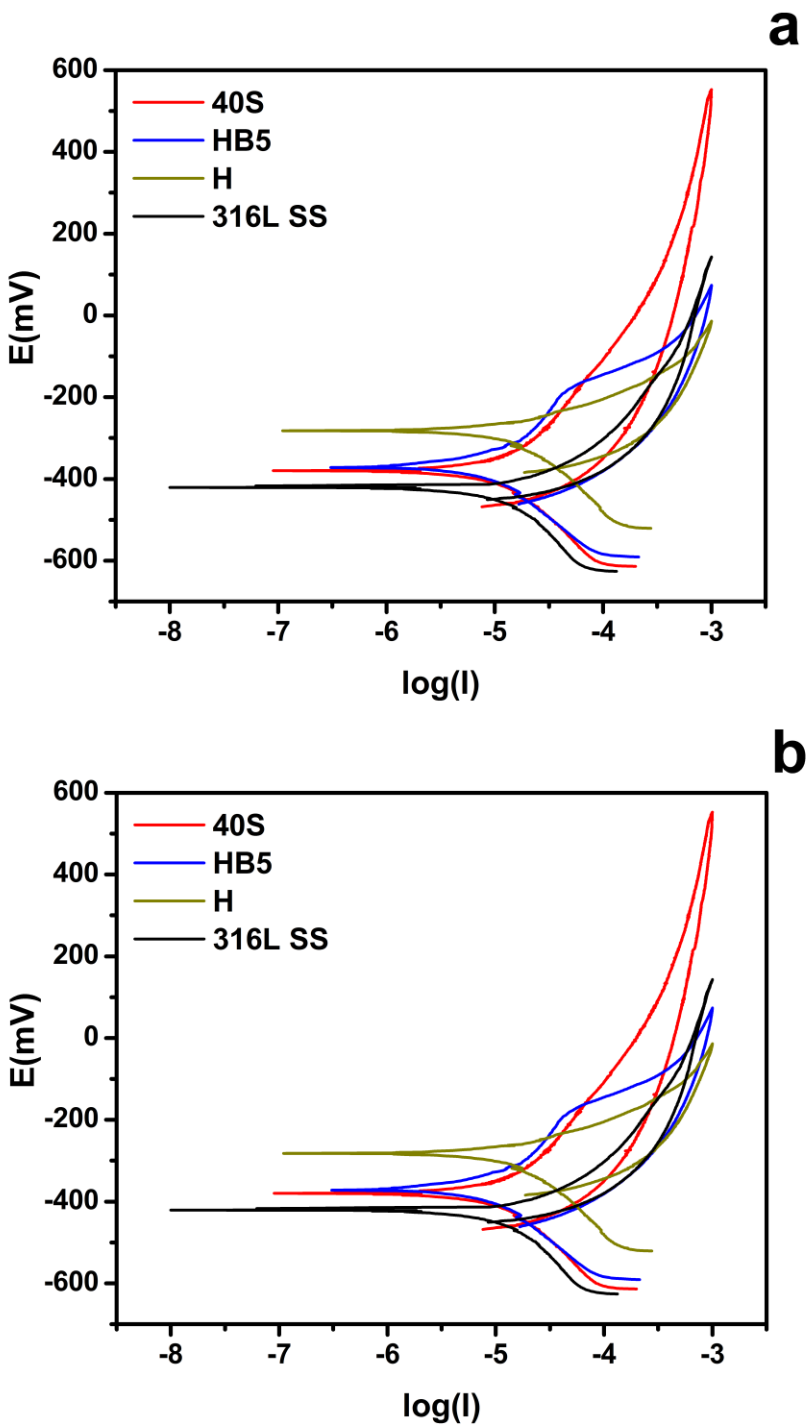

Figure 10. Potentiodynamic polarisation curves of 40S, HB5 and H samples compared to uncoated 316L SS in SBF (a) and DMEM (b) media.

3.7.2. Electrochemical impedance spectroscopic (EIS):

EIS is a powerful technique that is utilized to study the corrosion behaviour of metals or coated alloys. It provides a quantitative evaluation of corrosion properties of the system that would have been difficult using electrochemical measurements, as potentiostatic or potentiodynamic techniques. By appropriate interpretation of the EIS data based on an equivalent circuit (EC) model, the detailed information on the corrosion process at the electrolyte/electrode interface can be revealed. This technique is more effective for studying localized corrosion occurring through small pores. Representative EIS curves obtained from the coated sample compared to the uncoated substrate in SBF and DMEM solutions are shown in Figure 11 a, b. The figure shows that two-time constants, the first, capacitive loop at a medium frequency, and the second, a pseudo inductive loop at low frequency. The properties of the composites coating and their alteration can be determined at a higher frequency. The capacitive arcs usually result from charge transfer, coating layer effects and mass transfer [61]. Taking into account the physical structure of the electrode and its impedance response, the EC of the coated substrate/solution system is proposed and shown in Figure 12. (CC) represents the dielectric behaviour of the electrolyte/coating and, the constant phase element (CCPE) components. R_{por} is the resistance referred to the pore resistance. Oct is the Faraday charge transfer resistance due to the electrochemical reaction at the electrolyte/substrate interface, R_{sol} is set in a series with other elements of the circuit [62]. Figure 11 a-b shows Nyquist diagrams for substrate and composite coated samples in SBF and DMEM solutions. For the as-received condition, Nyquist plots obtained from EIS experimental data are shown together with data generated using EC that shown in Figure 12. The experimental data can be confirmed by the value given in Table 4. The total impedance $|Z|$ of uncoated substrate is $1.05x10^3$ Ωcm^2 in SBF and $1.12x10^3$ Ωcm^2 in DMEM solutions. These values are lower than that of coated composites that have total impedance of $8.7\ x10^4$, $8.08\ x10^4$, $5.8\ x10^4$ Ωcm^2 for 40S, HB5, H in SBF and $9.6\ x10^4$, $3.4\ x10^4$, $4.9\ x10^4$ Ωcm^2 in DMEM respectively for the same composites. Moreover, there is a decrease in capacitance values from $2.01x10^{-5}$ Fcm^{-2} for uncoated steel to $3.9x10^{-5}$, $3.9x10^{-5}$, and $5.1x10^{-5}$ Fcm^{-2} for H, HB5, 40S composites respectively in SBF solution, and from $1.74x10^{-5}Fcm^{-2}$to $3.72x10^{-5}$, $3.2x10^{-5}$, and $2.01x10^{-5}$ (Fcm^{-2}) for them in DMEM solution.

An increase in impedance and decrease in capacitance are observed when bioglass/chitosan composites coatings were present. Therefore, the surface acts as an active

barrier layer against corrosive ions and improving the corrosion resistance of the implant during the period under study [63, 64].

Table 4. Fitting parameters for uncoated substrate and coated composites samples in SBF and DMEM solution using the equivalent circuit in Figure 11

Biological solutions	**SBF**			**DMEM**		
parameters	R_{sol} (Ωcm^2)	$\|Z\|$ (Ωcm^2)	C (Fcm^{-2})	R_{sol}(Ωcm^2)	$\|Z\|$ (Ωcm^2)	C (Fcm^{-2})
SS316 Blank	**36**	**$1.05x10^3$**	**$2.01x10^{-5}$**	**13.71**	**$1.12x10^3$**	**$1.74x10^{-5}$**
40S	38	$8.7x10^4$	$5.1x10^{-5}$	15.67	$9.6x10^4$	$2.01x10^{-5}$
HB5	32	$8.08x10^4$	$3.9x10^{-5}$	15.8	$3.4x10^4$	$3.72x10^{-5}$
H	35	$5.8x10^4$	$3.9x10^{-5}$	13.5	$4.9x10^4$	$3.2x10^{-5}$

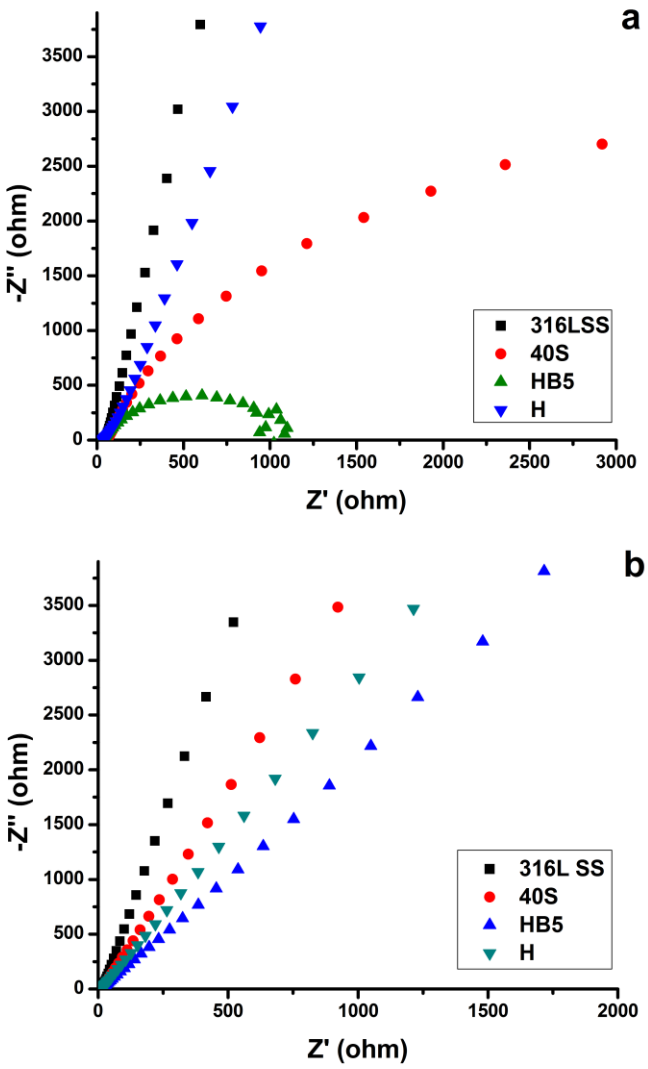

Figure 11. Nyquist curves in SBF solution (a), and in DMEM solution (b) for 40S, HB5 and H samples compared to uncoated 316L SS.

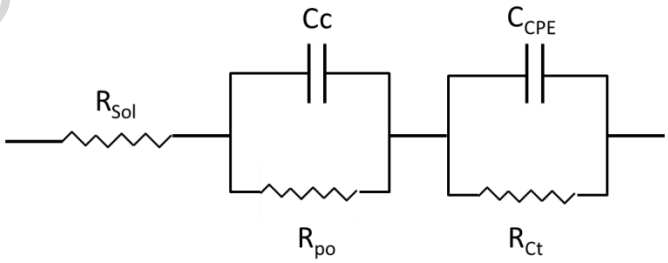

Figure 12. EC used in our EIS data analysis of 40S, HB5 and H coated samples on 316L stainless steel.

Conclusion

The silicate-based were incorporated in chitosan polymer as composite coatings for 316L SS using electrophoretic deposition (EPD). The glasses was designed by modification of Bioglass® by addition of boron, and Bioglass® was synthesized for comparison. The coating process were performed in aqueous solution, (green electrolyte) which is cost effective and possesses a good environmental impact. Different EPD parameters were tested to determine the optimum conditions for the coating process. The best composite coatings were achieved at 20 V, deposition time of 5 min, 0.5 g/l polymer concentration and 6 g/l glass concentration. The thermogravimetric analysis of different samples demonstrated that the total weight loss for different composite coatings (40S, HB5 and H) was 28.5, 25 and 31.5 wt %, respectively. Furthermore, XRD patterns of as-prepared glass samples showed that there were no diffraction peaks of all samples, which indicated the amorphous structure of the glasses. SEM micrographs of different coated substrates represented desirable and crack-free coatings. The measured contact angle of water drop on the coating surface showed a high wettability of composite coating layers, which mainly came from the hydrophilicity nature of chitosan polymer and bioactive glass particles. The composite coatings enhanced the bioactivity by forming bone-like apatite mineral on the substrate surface. It confirmed by SEM/EDX analysis and measurement of Ca and P ions concentrations in SBF. Moreover, it improved the corrosion resistance of the metal surface in different physiological solutions as confirmed by the electrochemical measurements and detection of Fe ion in the immersed solution.

Acknowledgements

The financial support of the present work within National Research Centre, Cairo, Egypt is appreciated. The authors acknowledge and thank Central Labs, National Research Centre, for providing measurement facilities applied in this research.

References

[1] Kose C, Kacar R. In Vitro Bioactivity and Corrosion Properties of Laser Beam Welded Medical Grade AISI 316L Stainless Steel in Simulated Body Fluid. INTERNATIONAL JOURNAL OF ELECTROCHEMICAL SCIENCE. 2016;11:2762-77.

[2] Goodman SB, Yao Z, Keeney M, Yang F. The future of biologic coatings for orthopaedic implants. Biomaterials. 2013;34:3174-83.

[3] Aro HT, Alm JJ, Moritz N, Mäkinen TJ, Lankinen P. Low BMD affects initial stability and delays stem osseointegration in cementless total hip arthroplasty in women: a 2-year RSA study of 39 patients. Acta orthopaedica. 2012;83:107-14.

[4] Xie J, Luan BL. Formation of hydroxyapatite coating using novel chemo-biomimetic method. Journal of Materials Science: Materials in Medicine. 2008;19:3211-20.

[5] Chew K-K, Zein SHS, Ahmad AL, McPhail DS, Abdullah MF. The electrochemical studies of the corrosion resistance behaviour of hydroxyapatite coatings on stainless steel fabricated by electrophoretic deposition. Journal of Industrial and Engineering Chemistry. 2013;19:1123-9.

[6] Sasaki M, Inoue M, Katada Y, Nishida Y, Taniguchi A, Hiromoto S, et al. Preparation and biological evaluation of hydroxyapatite-coated nickel-free high-nitrogen stainless steel. Science and Technology of Advanced Materials. 2016.

[7] Heimann RB. The challenge and promise of low-temperature bioceramic coatings: An editorial. Surface and Coatings Technology. 2016;301:1-5.

[8] Monsalve M, Lopez E, Ageorges H, Vargas F. Bioactivity and mechanical properties of bioactive glass coatings fabricated by flame spraying. Surface and Coatings Technology. 2015;268:142-6.

[9] Dou Y, Cai S, Ye X, Xu G, Huang K, Wang X, et al. 45S5 bioactive glass–ceramic coated AZ31 magnesium alloy with improved corrosion resistance. Surface and Coatings Technology. 2013;228:154-61.

[10] Seuss S, Heinloth M, Boccaccini AR. Development of bioactive composite coatings based on combination of PEEK, bioactive glass and Ag nanoparticles with antibacterial properties. Surface and Coatings Technology. 2016;301:100-5.

[11] Córdoba LC, Marques A, Taryba M, Coradin T, Montemor F. Hybrid coatings with collagen and chitosan for improved bioactivity of Mg alloys. Surface and Coatings Technology. 2017.

[12] Cordero-Arias L, Boccaccini A. Electrophoretic deposition of chondroitin sulfate-chitosan/bioactive glass composite coatings with multilayer design. Surface and Coatings Technology. 2017;315:417-25.

[13] Radda'a NS, Goldmann WH, Detsch R, Roether JA, Cordero-Arias L, Virtanen S, et al. Electrophoretic deposition of tetracycline hydrochloride loaded halloysite nanotubes chitosan/bioactive glass composite coatings for orthopedic implants. Surface and Coatings Technology. 2017;327:146-57.

[14] Montemor M. Functional and smart coatings for corrosion protection: a review of recent advances. Surface and Coatings Technology. 2014;258:17-37.

[15] Weiner S, Wagner HD. The material bone: structure-mechanical function relations. Annual Review of Materials Science. 1998;28:271-98.

[16] de Jonge LT, Leeuwenburgh SC, Wolke JG, Jansen JA. Organic–inorganic surface modifications for titanium implant surfaces. Pharmaceutical research. 2008;25:2357-69.

[17] Simchi A, Tamjid E, Pishbin F, Boccaccini A. Recent progress in inorganic and composite coatings with bactericidal capability for orthopaedic applications. Nanomedicine: Nanotechnology, Biology and Medicine. 2011;7:22-39.
[18] Hench LL, Splinter RJ, Allen W, Greenlee T. Bonding mechanisms at the interface of ceramic prosthetic materials. Journal of Biomedical Materials Research. 1971;5:117-41.
[19] Krause D, Thomas B, Leinenbach C, Eifler D, Minay EJ, Boccaccini AR. The electrophoretic deposition of Bioglass® particles on stainless steel and Nitinol substrates. Surface and Coatings Technology. 2006;200:4835-45.
[20] Schausten MC, Meng D, Telle R, Boccaccini AR. Electrophoretic deposition of carbon nanotubes and bioactive glass particles for bioactive composite coatings. Ceramics international. 2010;36:307-12.
[21] Naghib SM, Ansari M, Pedram A, Moztarzadeh F, Feizpour A, Mozafari M. Bioactivation of 304 stainless steel surface through 45S5 bioglass coating for biomedical applications. International Journal of Electrochemical Science. 2012;7:2890-903.
[22] Galliano P, De Damborenea JJ, Pascual MJ, Duran A. Sol-gel coatings on 316L steel for clinical applications. Journal of sol-gel science and technology. 1998;13:723-7.
[23] Fathi M, Doostmohammadi A. Bioactive glass nanopowder and bioglass coating for biocompatibility improvement of metallic implant. Journal of materials processing technology. 2009;209:1385-91.
[24] Xiao Y, Song L, Liu X, Huang Y, Huang T, Wu Y, et al. Nanostructured bioactive glass–ceramic coatings deposited by the liquid precursor plasma spraying process. Applied Surface Science. 2011;257:1898-905.
[25] Mehdipour M, Afshar A, Mohebali M. Electrophoretic deposition of bioactive glass coating on 316L stainless steel and electrochemical behavior study. Applied Surface Science. 2012;258:9832-9.
[26] Wang X, Wen C. Corrosion protection of mesoporous bioactive glass coating on biodegradable magnesium. Applied Surface Science. 2014;303:196-204.
[27] Omar S, Ballarre J, Ceré S. Protection and functionalization of AISI 316L stainless steel for orthopedic implants: hybrid coating and sol gel glasses by spray to promote bioactivity. Electrochimica Acta. 2016;203:309-15.
[28] Durand LAH, Vargas GE, Romero NM, Vera-Mesones R, Porto-López JM, Boccaccini AR, et al. Angiogenic effects of ionic dissolution products released from a boron-doped 45S5 bioactive glass. Journal of Materials Chemistry B. 2015;3:1142-8.
[29] Devirian TA, Volpe SL. The physiological effects of dietary boron. 2003.
[30] Wang H, Zhao S, Zhou J, Shen Y, Huang W, Zhang C, et al. Evaluation of borate bioactive glass scaffolds as a controlled delivery system for copper ions in stimulating osteogenesis and angiogenesis in bone healing. Journal of Materials Chemistry B. 2014;2:8547-57.
[31] Ameen HNM, Hussain SA, Ahmed ZA. Anti-inflammatory effects of boron alone or as adjuvant with dexamethasone in animal models of chronic and granulomatous inflammation. 2015.
[32] Boccaccini A, Peters C, Roether J, Eifler D, Misra S, Minay E. Electrophoretic deposition of polyetheretherketone (PEEK) and PEEK/Bioglass® coatings on NiTi shape memory alloy wires. Journal of materials science. 2006;41:8152-9.
[33] Cordero-Arias L, Cabanas-Polo S, Virtanen S, Boccaccini AR. Electrophoretic Deposition of Nanostructured Titania-Bioactive Glass/Alginate Coatings on Stainless Steel. Key Engineering Materials. 2015;654.

[34] Pishbin F, Simchi A, Ryan M, Boccaccini A. Electrophoretic deposition of chitosan/45S5 Bioglass® composite coatings for orthopaedic applications. Surface and Coatings Technology. 2011;205:5260-8.
[35] Pishbin F, Mouriño V, Gilchrist J, McComb D, Kreppel S, Salih V, et al. Single-step electrochemical deposition of antimicrobial orthopaedic coatings based on a bioactive glass/chitosan/nano-silver composite system. Acta biomaterialia. 2013;9:7469-79.
[36] Zhitomirsky D, Roether J, Boccaccini A, Zhitomirsky I. Electrophoretic deposition of bioactive glass/polymer composite coatings with and without HA nanoparticle inclusions for biomedical applications. Journal of materials processing technology. 2009;209:1853-60.
[37] Molaei A, Yari M, Afshar MR. Modification of electrophoretic deposition of chitosan–bioactive glass–hydroxyapatite nanocomposite coatings for orthopedic applications by changing voltage and deposition time. Ceramics International. 2015;41:14537-44.
[38] Clavijo S, Membrives F, Quiroga G, Boccaccini AR, Santillán MJ. Electrophoretic Deposition of Chitosan/Bioglass® and Chitosan/Bioglass®/TiO 2 Composite Coatings for Bioimplants. Ceramics International. 2016.
[39] Rabea EI, Badawy ME-T, Stevens CV, Smagghe G, Steurbaut W. Chitosan as antimicrobial agent: applications and mode of action. Biomacromolecules. 2003;4:1457-65.
[40] Chatelet C, Damour O, Domard A. Influence of the degree of acetylation on some biological properties of chitosan films. Biomaterials. 2001;22:261-8.
[41] Zhang BG, Myers DE, Wallace GG, Brandt M, Choong PF. Bioactive coatings for orthopaedic implants—recent trends in development of implant coatings. International journal of molecular sciences. 2014;15:11878-921.
[42] Besra L, Liu M. A review on fundamentals and applications of electrophoretic deposition (EPD). Progress in materials science. 2007;52:1-61.
[43] Boccaccini A, Keim S, Ma R, Li Y, Zhitomirsky I. Electrophoretic deposition of biomaterials. Journal of the Royal Society Interface. 2010;7:S581-S613.
[44] Fiorilli S, Baino F, Cauda V, Crepaldi M, Vitale-Brovarone C, Demarchi D, et al. Electrophoretic deposition of mesoporous bioactive glass on glass–ceramic foam scaffolds for bone tissue engineering. Journal of Materials Science: Materials in Medicine. 2015;26:21.
[45] Molino G, Bari A, Baino F, Fiorilli S, Vitale-Brovarone C. Electrophoretic deposition of spray-dried Sr-containing mesoporous bioactive glass spheres on glass–ceramic scaffolds for bone tissue regeneration. Journal of Materials Science. 2017:1-12.
[46] Miola M, Verné E, Piredda A, Seuss S, Cabanas-Polo S, Boccaccini AR. Development and Characterization of PEEK/B2O3-Doped 45S5 Bioactive Glass Composite Coatings Obtained by Electrophoretic Deposition. Key Engineering Materials: Trans Tech Publ; 2015. p. 165-9.
[47] Kokubo T, Takadama H. How useful is SBF in predicting in vivo bone bioactivity? Biomaterials. 2006;27:2907-15.
[48] Simchi A, Pishbin F, Boccaccini A. Electrophoretic deposition of chitosan. Materials Letters. 2009;63:2253-6.
[49] Cabanas-Polo S, Boccaccini AR. Understanding Bioactive Glass Powder Suspensions for Electrophoretic Deposition of Bioactive Glass-Polymer Coatings. Journal of The Electrochemical Society. 2015;162:D3077-D83.

[50] Roach P, Eglin D, Rohde K, Perry CC. Modern biomaterials: a review—bulk properties and implications of surface modifications. Journal of Materials Science: Materials in Medicine. 2007;18:1263-77.
[51] Hassan MM. Binding of a quaternary ammonium polymer-grafted-chitosan onto a chemically modified wool fabric surface: assessment of mechanical, antibacterial and antifungal properties. RSC Advances. 2015;5:35497-505.
[52] Kaiser J-P, Bruinink A. Investigating cell–material interactions by monitoring and analysing cell migration. Journal of Materials Science: Materials in Medicine. 2004;15:429-35.
[53] Rohanová D, Boccaccini AR, Horkavcová D, Bozděchová P, Bezdička P, Častorálová M. Is non-buffered DMEM solution a suitable medium for in vitro bioactivity tests? Journal of Materials Chemistry B. 2014;2:5068-76.
[54] Hench LL. Bioceramics: from concept to clinic. Journal of the american ceramic society. 1991;74:1487-510.
[55] Hill R. An alternative view of the degradation of bioglass. Journal of Materials Science Letters. 1996;15:1122-5.
[56] Mucha M, Pawlak A. Complex study on chitosan degradability. POLIMERY-WARSAW-. 2002;47:509-16.
[57] Ma G, Yang D, Kennedy JF, Nie J. Synthesize and characterization of organic-soluble acylated chitosan. Carbohydrate Polymers. 2009;75:390-4.
[58] Dietrich E, Oudadesse H, Lucas-Girot A, Mami M. In vitro bioactivity of melt-derived glass 46S6 doped with magnesium. Journal of Biomedical Materials Research Part A. 2009;88:1087-96.
[59] Pourhashem S, Afshar A. Double layer bioglass-silica coatings on 316L stainless steel by sol–gel method. Ceramics International. 2014;40:993-1000.
[60] Kheirkhah M, Fathi M, Salimijazi HR, Razavi M. Surface modification of stainless steel implants using nanostructured forsterite (Mg 2 SiO 4) coating for biomaterial applications. Surface and Coatings Technology. 2015;276:580-6.
[61] Xin Y, Liu C, Zhang W, Jiang J, Tang G, Tian X, et al. Electrochemical Behavior Al2O3⁄Al Coated Surgical AZ91 Magnesium Alloy in Simulated Body Fluids. Journal of the Electrochemical Society. 2008;155:C178-C82.
[62] Zhang Y, Yan C, Wang F, Li W. Electrochemical behavior of anodized Mg alloy AZ91D in chloride containing aqueous solution. Corrosion Science. 2005;47:2816-31.
[63] Gopi D, Prakash VCA, Kavitha L, Kannan S, Bhalaji P, Shinyjoy E, et al. A facile electrodeposition of hydroxyapatite onto borate passivated surgical grade stainless steel. Corrosion Science. 2011;53:2328-34.
[64] Vijayalakshmi U, Chellappa M, Anjaneyulu U, Manivasagam G, Sethu S. Influence of coating parameter and sintering atmosphere on the corrosion resistance behavior of electrophoretically deposited composite coatings. Materials and Manufacturing Processes. 2016;31:95-106.

Highlights

- Two bioactive glass/chitosan composite coatings are prepared and electrophoretically deposited in aqueous (green) electrolyte solution on 316L SS.
- Deposition parameters of the composite coatings are fully investigated and optimized .
- Bioactive glass composites coated 316L stainless steel are characterized and evaluated in SBF and DMEM solutions to determine its in-vitro bioactivity.
- Potentiodynamic polarization and EIS techniques are used to estimate the corrosion protection of coated 316L SS in SBF and DMEM solutions.
- These coats will be used in further study as a delivery of antibacterial agents.